nature physics

ARTICLES

https://doi.org/10.1038/s41567-019-0436-5

Turning a molecule into a coherent two-level quantum system

Daqing Wang[1,3], Hrishikesh Kelkar[1,3], Diego Martin-Cano[1], Dominik Rattenbacher[1], Alexey Shkarin[1], Tobias Utikal[1], Stephan Götzinger[1,2] and Vahid Sandoghdar[1,2]*

The use of molecules in quantum optical applications has been hampered by incoherent internal vibrations and other phononic interactions with their environment. Here we show that an organic molecule placed into an optical microcavity behaves as a coherent two-level quantum system. This allows the observation of 99% extinction of a laser beam by a single molecule, saturation with less than 0.5 photons and non-classical generation of few-photons super-bunched light. Furthermore, we demonstrate efficient interaction of the molecule–microcavity system with single photons generated by a second molecule in a distant laboratory. Our achievements represent an important step towards linear and nonlinear quantum photonic circuits based on organic platforms.

Molecules provide very compact quantum systems that host well defined transitions, ranging from the microwave to the ultraviolet domains associated with their rotational, vibrational and electronic states. In addition, these intrinsic mechanical and electronic degrees of freedom can be coupled through various well defined transitions and selection rules. Indeed, molecular systems have attracted renewed attention within the community of quantum physics both in the gas[1,2] and condensed[3–9] phases. In the former case, molecules possess long-lived vibrational levels and well resolved rotational transitions, but their cooling and trapping are difficult, so access to single molecules has only very recently been explored[10]. On the other hand, addressing single molecules in solids has been feasible with high spatial and spectral resolutions for nearly three decades, but a substantial degree of decoherence remains in this system owing to phononic couplings[11].

The ground vibrational level of the electronic excited state ($|e, v=0\rangle$) in a dye molecule can couple to $|g, v=0\rangle$ and $|g, v\neq 0\rangle$ in the ground state following the Franck–Condon principle (Fig. 1a). When embedded in a solid, each of these transitions entails a zero-phonon line (ZPL) and a phonon wing caused by coupling to matrix phonons (the Debye–Waller factor). In the case of polycyclic aromatic hydrocarbons (PAHs), the ZPL connecting $|g, v=0\rangle$ and $|e, v=0\rangle$ (00ZPL) can be narrowed by about 10^5-fold to the Fourier limit when cooled to liquid-helium temperatures. Nevertheless, the decay of $|e, v=0\rangle$ via $|g, v\neq 0\rangle$ levels and the subsequent fast relaxation of the latter states give rise to decoherence, making phase-sensitive and nonlinear quantum operations inefficient[12,13]. One way to counter this decoherence is to enhance the 00ZPL in a selective manner and thus modify the branching ratio out of $|e, v=0\rangle$.

In the past decade there have been many efforts to enhance the radiative properties of molecules with plasmonic nanostructures[6,14]. However, the large bandwidth of plasmon resonances does not allow for selective addressing of narrow transitions. To remedy this, one can use optical microcavities to enhance molecular ZPLs with a substantial Purcell factor, $F=\frac{3}{4\pi^2}\frac{Q\lambda^3}{V}\gg 1$ (ref. [15]). First attempts in this direction have been reported[16–19], but the results fall short of notable enhancements. A successful laboratory realization needs to consider and tackle several technical issues, especially in regard to the microcavity design. While monolithic microcavities are fairly robust, they have limited tunability and may be affected by difficulties in the positioning of emitters. Open Fabry–Perot resonators, on the other hand, are difficult to stabilize in the cryostat but are conveniently adjustable and can be more easily combined with various materials. In this Article, we make use of an open, tunable and laterally scannable Fabry–Perot microcavity with very small mode volume (V) and moderate quality factor (Q)[19–21].

Experimental

The method of choice for selecting single quantum emitters embedded in a solid is to exploit the inherent spectral inhomogeneity of such a system[11]. By operating at low enough temperatures, the homogeneous linewidths of individual emitters become so narrow that they no longer overlap. Thus, a narrowband laser beam can address the 00ZPLs of the various emitters located in the illumination volume one by one. In our experiment, we used dibenzoterrylene (DBT), of the PAH family, embedded in a thin anthracene (AC) crystal (Fig. 1a). The 00ZPL of DBT:AC lies in the interval 783–785 nm and can become as narrow as its Fourier limit of about 40 MHz at $T\lesssim 4$ K (ref. [22]). To produce a Fabry–Perot cavity, we fabricated a curved micromirror at the end of an optical fibre and used a planar mirror[19,21], both coated with a dielectric multilayer (Fig. 1b,c). In Fig. 1d we present an overview of the experimental arrangement. Details of the set-up and the microcavity characterization are provided in the Methods.

Results

Transmission and reflection of a laser beam. The presence of an emitter inside a cavity modifies the interference of the fields that result from the reflections between its mirrors. To probe the intracavity field, we exploited the cross-polarized reflection (CPR) from the cavity, providing a measure equivalent to a transmission recording[19] (see Methods). The blue symbols in Fig. 2a display a CPR spectrum in the absence of coupling to a molecule, and the blue solid curve shows a fit to these data using a Voigt profile.

[1]Max Planck Institute for the Science of Light, Erlangen, Germany. [2]Department of Physics, Friedrich Alexander University, Erlangen, Germany. [3]These authors contributed equally: Daqing Wang, Hrishikesh Kelkar. *e-mail: vahid.sandoghdar@mpl.mpg.de

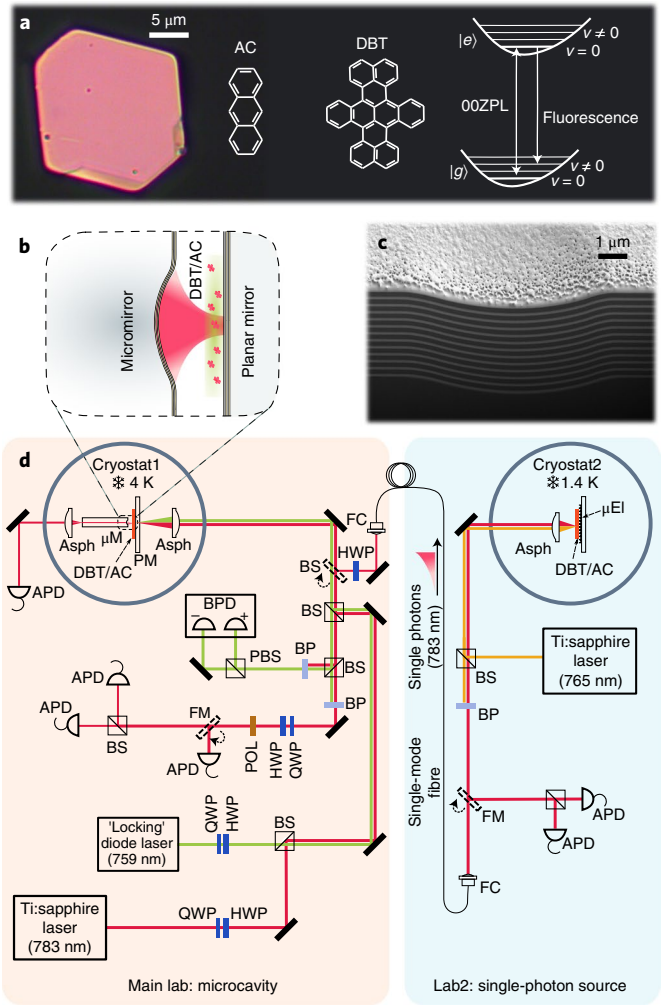

Fig. 1 | Schematics of the experimental arrangements. a, Optical microscope image of a thin anthracene (AC) crystal, its molecular structures together with that of dibenzoterrylene (DBT), and the energy level scheme of the latter. **b**, Sketch of molecules embedded in a thin AC crystal placed in a microcavity. **c**, Electron microscope cross-sectional image of the multilayer coating of the curved micromirror with radius of curvature of 10 μm after being cut by a focused ion beam. The apparent surface roughness is caused by the metallic coating necessary for electron microscopy and is absent on the mirror used in the measurements. **d**, Overview of the experimental set-ups in two different laboratories. See Methods for details. μEl, ITO microelectrodes; APD, avalanche photodiode; BPD, balanced photodetector; PBS, polarizing beamsplitter; Asph, aspheric lens; BS, beamsplitter; FM, flip mirror; FC, fibre coupler; POL, polarizer; HWP, half-waveplate; QWP, quarter-waveplate; BP, narrowband interference filter; μM, micromirror; PM, planar mirror.

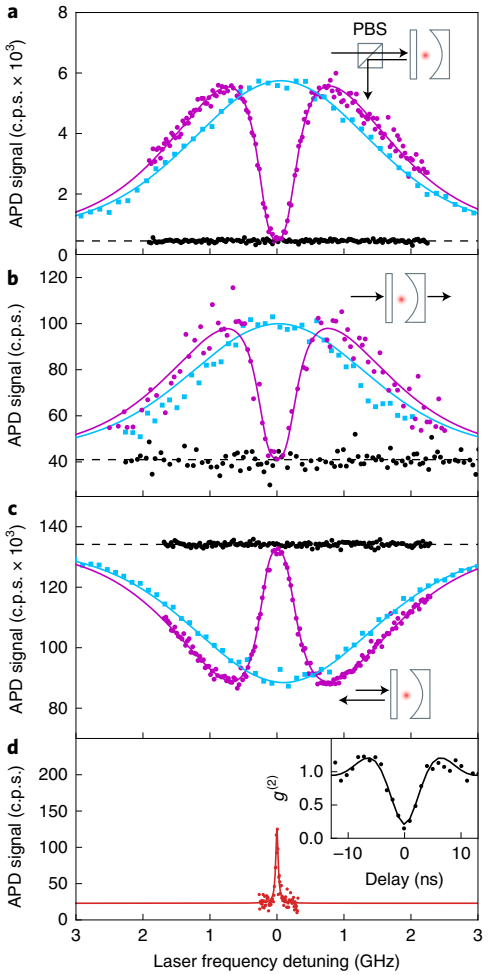

Fig. 2 | Resonant response of the molecule–microcavity composite to a laser beam. a, Transmission spectra of the cavity with (magenta) and without (blue) the molecular contribution in units of counts per second (c.p.s.). The measurements were performed in cross-polarized mode. Black symbols show the intensity of the laser beam when the cavity resonance was detuned by about 20 GHz, acting as a reference level. A single molecule interrupts the cavity transmission by 99%. **b**, Same as in **a** but for direct transmission through the micromirror fabricated at the end of the optical fibre. **c**, Reflection spectra recorded on the same molecule as in **a** and **b**. **d**, Fluorescence excitation spectrum of the same molecule recorded far detuned from the cavity resonance. The inset shows the second-order intensity autocorrelation function, verifying that this light is antibunched. See main text for an explanation of the theoretical fits (solid curves).

The black symbols in this figure represent a reference CPR signal when the cavity frequency was detuned by about 20 GHz.

To examine the effect of a single molecule on the optical response of the microcavity, we tuned the resonance of the latter through the inhomogeneous band of DBT:AC and searched for the signature of molecular resonances directly in the cavity CPR spectrum while scanning the laser frequency. The magenta symbols in Fig. 2a present an example where the cavity transmission drops by 99% when it becomes resonant with a single molecule. In Fig. 2b, we also display a direct transmission measurement recorded through the micromirror (Fig. 1d). All features in Fig. 2a,b agree, as confirmed by the high quality of the fits using common parameters. However, the signal-to-noise ratio (SNR) is lower in Fig. 2b because the numerical aperture of the single-mode fibre holding the micromirror does not match the cavity mode, thus resulting in a weak signal.

Next, we investigated the remarkably large effect of a single molecule on an incident laser beam further by measuring the direct reflection of the system. The blue symbols in Fig. 2c show the central part of the cavity resonance measured in the absence of molecular coupling. We note that the cavity resonance does not dip to zero due to mode mismatch, slight impedance mismatch introduced by the AC crystal and remaining vibrations. Nevertheless, the magenta symbols show that when the cavity is brought into resonance with a single molecule, the reflection dip vanishes. We shall present a quantitative discussion of the spectra in Fig. 2a–c as well as the solid theory curves used to fit them in the next section.

Cavity quantum electrodynamics modifications and spectral analysis. The data in Fig. 2a–c let us deduce the full-width at half-maximum (FWHM) of the molecular 00ZPL to be 604 ± 21 MHz under coupling to the microcavity. To determine the linewidth of the very same molecule without the influence of the cavity, we detuned the resonance of the latter and recorded a redshifted fluorescence signal from the molecule as a function of the excitation frequency. The outcome shown in Fig. 2d reveals FWHM $= 44 \pm 5$ MHz, which is in the range of the values for the bulk DBT:AC system[22]. The weaker signal in this case stems from the difficulty of extracting the broad fluorescence through the higher-order transverse modes of the cavity. Photon antibunching of the fluorescence signal recorded via intensity autocorrelation ($g^{(2)}(\tau)$) confirms that it originates from only one molecule (inset of Fig. 2d).

The linewidth of an unperturbed molecule can be expressed as $\gamma^0 = \gamma^0_{\mathrm{zpl}} + \gamma_{\mathrm{red}}$, where γ^0_{zpl} stands for the decay rate of the excited state $|e, v=0\rangle$ into the 00ZPL channel, and γ_{red} denotes the contributions of all redshifted emission, including phonon wings and vibrational decay paths. When the cavity is resonant with the 00ZPL, the component of γ^0_{zpl} emitted into the cavity mode is enhanced by Purcell factor F, yielding $\gamma'_{\mathrm{zpl}} = (1+F)\gamma^0_{\mathrm{zpl}}$. Hence, considering that $\gamma_{\mathrm{red}} \approx 2\gamma^0_{\mathrm{zpl}}$ for DBT:AC[23], we can write the modified decay rate of the excited state as $\gamma' = \gamma_{\mathrm{red}} + \gamma'_{\mathrm{zpl}} = (3+F)\gamma^0_{\mathrm{zpl}}$. We thus deduce from our experimental findings of $\gamma^0/2\pi = 44 \pm 5$ MHz and $\gamma'/2\pi = 604 \pm 21$ MHz a Purcell factor of $F = 38 \pm 5$.

A very useful measure for the efficiency of emitter–cavity coupling is the β factor, defined as the ratio of the power emitted into the cavity mode and the total emitted power[24]. The β factor associated with an ideal two-level atom can be computed as $\frac{F}{F+1}$ and would correspond to $97.4 \pm 0.3\%$ for our cavity. To assess the overall degree of coherence, one also has to account for losses through the redshifted channels, arriving at $\beta = \frac{\gamma^0_{\mathrm{zpl}} F}{\gamma'} = \frac{F}{F+3} = 93\%$.

The strong modification of the molecular emission on the 00ZPL changes its branching ratio α, defined as the fraction of the power in the 00ZPL to the overall emission from the excited state. Our results demonstrate a modification from $\alpha \approx 33\%$ for bulk DBT:AC to $\alpha' = \frac{\gamma'_{\mathrm{zpl}}}{\gamma'} = \frac{F+1}{F+3} = 95\%$ in the cavity. This implies that we have successfully converted a molecule to a two-level quantum system to within 95%. The obtained high values of α and β have immediate consequences for the efficiency of coherent linear and nonlinear processes at the single-molecule level[12,13].

To investigate the radiative modifications further, we took advantage of the axial tunability of our microcavity and recorded a series of CPR spectra at different molecule–cavity frequency detunings. Figure 3a demonstrates the evolution of the molecule–cavity spectral modifications, providing a wealth of quantitative data and a thorough comparison between experiment and theory. In a first simple approach, we fit the observed Fano-like dispersive line shapes using a generalized Lorentzian function. Figure 3b nicely traces the linewidth of the molecular resonance (left vertical axis) and the corresponding Purcell factor (right vertical axis) as a function of the cavity frequency detuning. The data in Fig. 3a can also be analysed by considering a rigorous theory that treats the interaction of an incoming field with both the molecule and the cavity on the same footing[25]. The solid curves in Figs. 2a–c and 3a show fits to the experimental data with excellent agreement using such a model (see Supplementary Information).

Next, we analysed the influence of the cavity coupling on the centre frequency of the molecular resonance. Figure 3c plots the latter as a function of the cavity–molecule frequency detuning and reveals frequency shifts by up to about ± 150 MHz towards blue or red, depending on the sign of the detuning. This can be interpreted as a change in the contribution of vacuum fluctuations to the absolute value of the 00ZPL, in other words, of the Lamb shift[15,26]. The correction disappears when the cavity is resonant with the molecular line and peaks at the largest slope of the resonance profile. This behaviour is similar to the well known AC Stark shift proportional to the laser–atom detuning[27].

To place our parameters in the context of weak and strong coupling regimes, in Fig. 3e–i we present calculated transmission (green) and fluorescence (red) spectra for various cavity linewidths. While the fluorescence spectra clearly show the onset of a line splitting for higher finesse cavities, the splitting between the maxima in the transmission spectrum is nearly independent of the cavity finesse (dashed vertical lines). The symbols in Fig. 3g show that the experimental data correspond to the transitional regime where the spectrum changes its character from a molecular extinction dip on a broad cavity resonance to one with two split polaritonic resonance profiles at par. The fluorescence spectrum in this region is shortly before bifurcation into two maxima, a signature of strong coupling[15]. For our system (with $\kappa \gg \gamma^0$), the onset of strong coupling can be quantitatively attributed to the regime where the cavity–molecule coupling rate g becomes larger than its value at the exceptional point, $g_{\mathrm{ep}} = \kappa/4$ (ref. [28]). To determine g for our experiment, in Fig. 3d we plot the frequencies of the two maxima that arise in the spectra of Fig. 3a. The splitting at zero detuning directly equals $2g$ (see Supplementary Information), yielding $g = 0.79 \pm 0.3$ GHz. Comparison of this value with $g_{\mathrm{ep}} = 0.82$ GHz computed for our system confirms that our experiment is situated right at the onset of strong coupling.

A convenient parameter that connects g, κ and γ is the cooperativity factor $C = \frac{4g^2}{\kappa\gamma}$. To estimate C, we use the total decay rate γ^0 so as to account for the internal loss of coherence through the redshifted emission paths, arriving at $C = 12.7$. We note that, in fact, our microcavity values of Q and V let us expect a much higher Purcell factor $F \approx 350$ and, thus, even stronger couplings than reported here. We attribute the discrepancy between the measured and predicted Purcell factors to the suboptimal position and orientation of the molecule with respect to the cavity electric field (see Supplementary Information).

Phase shift. The phase shift imprinted by a quantum emitter on a light beam can report on the state of the emitter in a non-destructive fashion. Previous experiments have demonstrated phase shifts of about 3° applied to a focused laser beam by single molecules in a crystal[12]. To explore this effect, we examined the CPR of a laser beam from the cavity, following the protocol described in ref. [12] and extracted the phase shift on the laser beam according to the procedure described in the Methods and the Supplementary Information.

The black symbols in Fig. 4 show the phase shift affected by the microcavity alone as the laser frequency was scanned across its resonance in the absence of a molecule. The red symbols in that figure display the recorded phase shift of the laser beam under the influence of a single molecule. The solid and dashed curves signify theoretical fits with and without the consideration of power broadening, respectively, allowing us to deduce phase shifts up to $\phi = \pm 66°$.

Photon bunching and single-photon nonlinearity. The photon statistics of a laser beam and of a quantum emitter take on very different forms, characterized by intensity autocorrelations $g^{(2)}(\tau) = 1$ and $g^{(2)}(0) = 0$, respectively. We now show that an efficient coupling between laser light and a molecule can result in highly non-trivial statistics of the emerging photons[29]. Figure 5a,c,e and g presents $g^{(2)}(\tau)$ measurements on a laser beam after interaction with the molecule–cavity system at different frequency detunings (Fig. 5b,d and f). The outcome $g^{(2)}(\tau) = 1$ in Fig. 5a reveals that the lower polariton branch in this case (Fig. 5b) has a laser-like nature. The measurement shown in Fig. 5c, on the other hand, presents a non-trivial case of

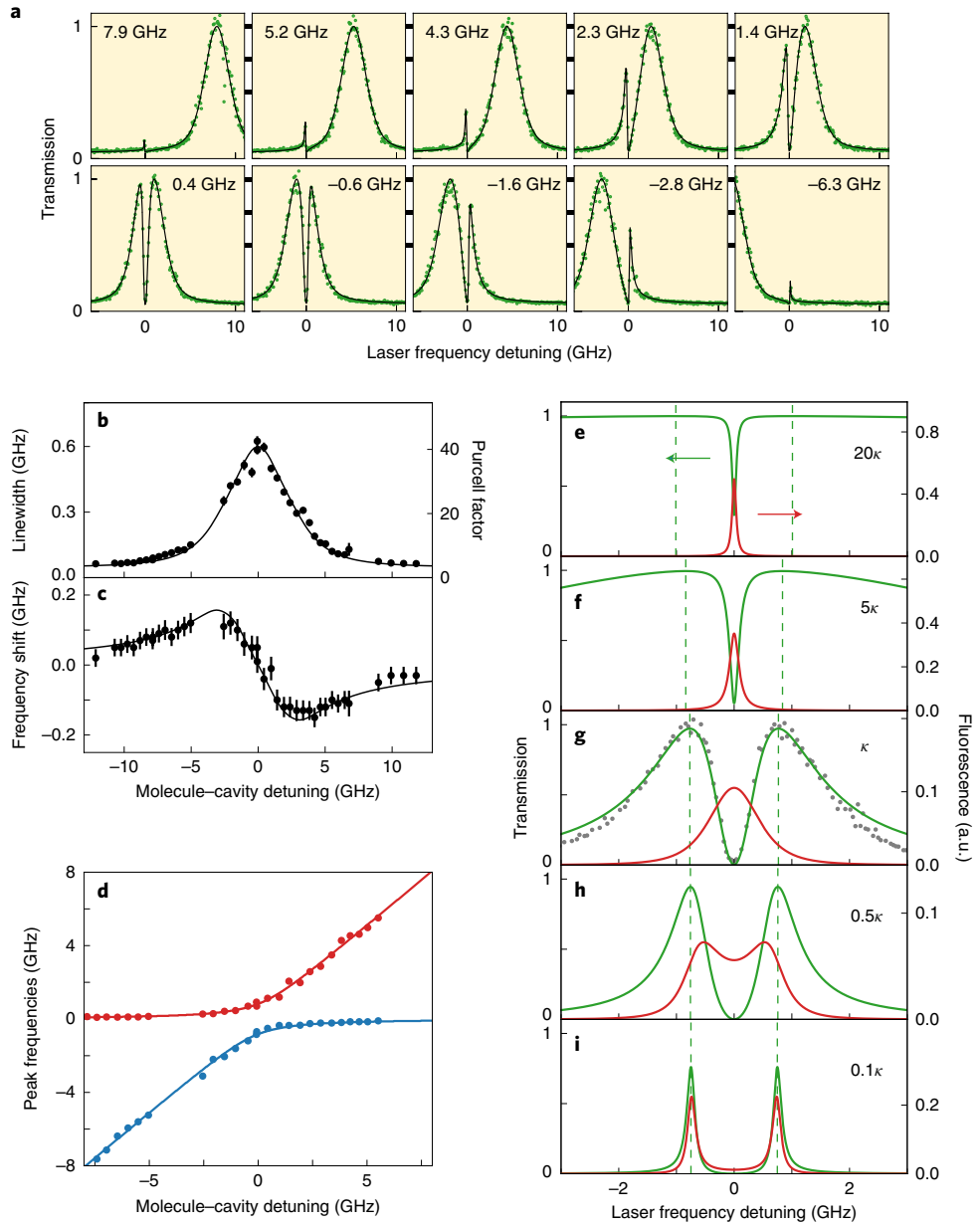

Fig. 3 | Frequency-detuned response of the molecule–cavity system. a, Series of transmission spectra for the given different molecule–cavity frequency detunings. **b**, Linewidth of the molecular resonance (left axis) and measured Purcell factor (right axis) as a function of molecule–cavity frequency detuning. **c**, Frequency shift of the molecular resonance (the modified Lamb shift) as a function of molecule–cavity frequency detuning. Error bars denote standard deviations. **d**, Positions of the peaks in the transmission spectrum as a function of molecule–cavity frequency detuning. All symbols in **a** to **d** present measured data while the solid curves show fits obtained from rigorous theoretical calculations. **e**–**i**, Calculated transmission (green) and fluorescence (red) spectra of a resonantly coupled system for $\gamma^0/2\pi = 44$ MHz and decreasing degree of cavity loss. Each panel denotes the cavity FWHM in terms of our experimental linewidth κ. The symbols in **g** represent the experimental CPR spectrum. The fit quality here is not as good because the contribution of vibrations to a Voigt profile are not taken into account in the calculated spectra. The dashed vertical lines display the positions of the maxima in the transmission spectra.

antibunching for the molecule-like branch of the spectrum in Fig. 5d. This antibunching results from the non-classical interference of the molecular scattering with the intracavity field and provides evidence for the dipole quadrature squeezing, which was recently detected in cavities[30] and in free space[31].

Figure 5e shows that tuning the laser frequency by a bit more than a linewidth (see Fig. 5f) changes the behaviour completely to a bunching effect. This phenomenon stems from the selective scattering of single-photon components from the Poisson distribution of photons in the incident laser beam[29], yielding a super-bunched few-photon state[32]. As displayed in Fig. 5g, this effect is maximized at the centre of the resonant molecule–cavity spectrum shown in Fig. 2a. Fitting the data by the theoretical model described in ref. [33] (see Supplementary Information) and using the cavity quantum electrodynamics parameters deduced from the spectral measurements let us deduce $g^{(2)}(0) = 21$, which is among the largest photon bunchings reported so far for a single emitter[34,35]. In fact, calculations in Fig. 5h show that for $C = 12.7$ one expects $g^{(2)}(0)$ to reach as high as 2.5×10^4 if the molecule, cavity and laser frequencies coincide. The discrepancy with the measured value of 21 is due to the limited detector response time of 50 ps and the residual background light (see Supplementary Information).

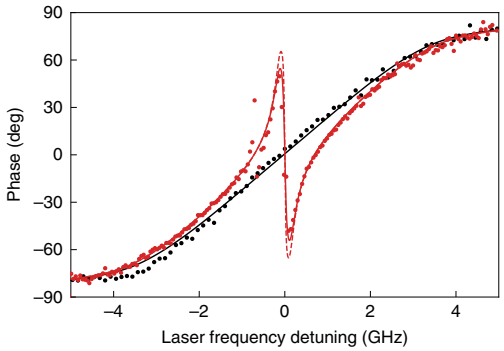

Fig. 4 | Large phase shift of a laser beam by a single molecule. Measured phase shifts of a laser beam after interacting with a cavity without (black symbols) and with (red symbols) a single molecule. The curves show the theoretical fits (see main text and Methods for details).

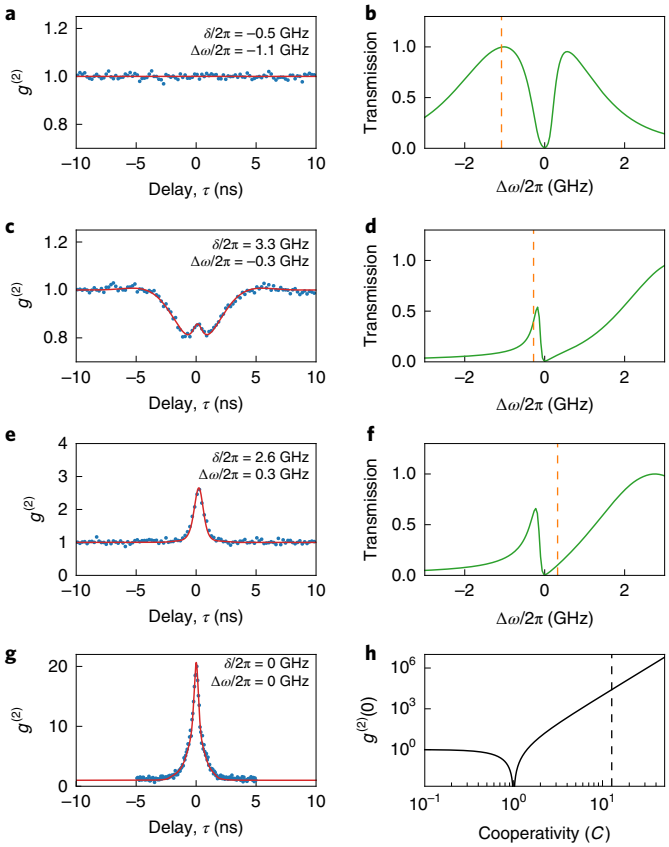

Fig. 5 | Strong modification of photon statistics. a, **c**, **e**, Intensity autocorrelation $g^{(2)}(\tau)$ of the CPR of a laser beam from the molecule–cavity composite for different molecule–cavity and laser frequencies. Molecule–cavity detuning (δ) and laser–molecule detuning ($\Delta\omega$) are displayed as legends in each plot. **b**, **d**, **f**, CPR spectra corresponding to the measurements shown in **a**,**c** and **e**. Orange dashed lines denote the laser frequency in each case. **g**, Photon bunching corresponding to $g^{(2)}(0) = 21$ at the molecular resonance in the set-up of Fig. 2. Red curves in **a**–**g** show theoretical fits. **h**, Theoretical predictions of $g^{(2)}(0)$ as a function of cooperativity C. The dashed line depicts the experimental parameter used in **g**.

The underlying mechanism of the phenomena observed above is that the molecule responds to only one photon at a time. This feature is also responsible for the intrinsic nonlinearity of an atom or molecule, which in turn leads to saturation as the excitation power is increased. We studied the nonlinear response of the cavity-coupled molecule by examining the extinction signal[36] (see Supplementary Information). We find that we reach the saturation parameter of $S = 1$ for a very low power of 420 pW coupled to the cavity, corresponding to only 0.44 photons per excited state lifetime of 264 ps. This result indicates that the operation regime of our experiment not only provides nearly perfect coupling in the weak excitation limit, but it also opens doors for efficient few-photon nonlinear operations[13,37].

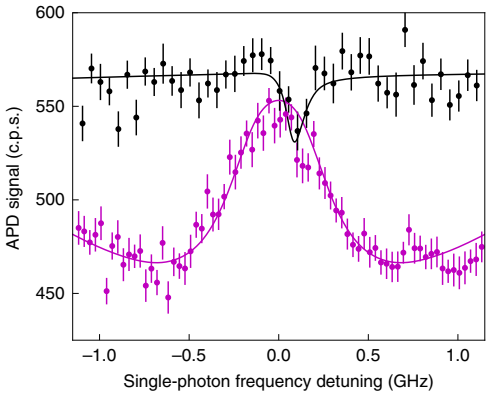

Fig. 6 | Reflection of single photons. Reflection spectrum of the molecule–cavity system when single photons from another molecule in a different laboratory impinged on it (magenta). Single photon budget: 6,000 c.p.s. out of the fibre in the microcavity lab, 3,000 c.p.s. incident onto the cavity, 500 c.p.s. on the final detector. The black symbols show a spectrum recorded when the cavity resonance was detuned by 6 GHz. Error bars show the level of shot noise. Note that our freedom to change the frequency of the single photons via the Stark effect on the 'source' molecule is limited compared to the case of a laser beam in Fig. 2. The small dip that is slightly shifted from the origin denotes the interference of the photons scattered by the target molecule with the component directly reflected at the flat mirror. See Supplementary Information for more details.

Wiring single photons to a single molecule. The ultimate frontier of light–matter interaction requires efficient coupling, or 'wiring' of a single photon to a single quantum emitter. To demonstrate such an exemplary experiment, we used a second molecule located in a different laboratory (Fig. 1d) as a source of narrowband single photons (see ref. [38] and Supplementary Information for details). The resulting stream of 30,000 photons per second with a FWHM linewidth of 41 MHz was coupled to a single-mode fibre and sent to the laboratory housing the microcavity. The magenta symbols in Fig. 6 present the reflection spectrum of this single-photon stream when the cavity was tuned to resonance with the 00ZPL of the 'target' molecule. While the count rate and the shot-noise-limited SNR are lower, the signal reproduces our findings in Fig. 2c, verifying that we also reach a high efficiency in coupling a molecule to single photons. We note in passing that one of the challenges in this experiment concerns tuning the frequency of single photons, which we realized via the Stark effect on the 'source' molecule. More discussion of the technical details and the reference spectrum shown by the black symbols in Fig. 6 is provided in the Supplementary Information.

In future, the degree of mastery demonstrated here can be combined with pulsed excitation of the source molecule and extended to the coupling of two or more photons to a single molecule[13,37]. Such an experiment establishes a platform for nonlinear quantum optics at its most fundamental level for the realization of gates and for quantum information processing[39].

Discussion and outlook

The large phase shift, nonlinearity at the single-photon level and strongly non-classical photon statistics demonstrated in this work give access to a range of quantum functionalities such as photon sorting and gates[39,40] in organic materials. In a next step, chip-based ring resonators[41] and nanoguides[42] will apply these opportunities to nanophotonic circuits. Having reached a highly efficient level of interaction between single photons and single molecules, one can then devise novel linear and nonlinear cooperative effects and polaritonic states, where a controlled number of molecules and photons are coupled via a common photonic mode along the circuit[43,44]. The practical implementation of these concepts would particularly benefit from the use of polymer media instead of organic crystals for device fabrication. Indeed, the Purcell enhanced radiative rates achieved in our work already compete with and dominate phonon-induced dephasing rates in polymers, which lie in the range of 0.1–1 GHz (ref. [45]). In addition to their immediate potential for large-scale organic quantum networks, we expect the selective modification of molecular rates demonstrated in this work to find applications in cooling and trapping of molecules in the gas phase, where closed transitions are desirable[46] and in control of molecular photochemical processes such as photochromic switching[5].

Online content

Any methods, additional references, Nature Research reporting summaries, source data, statements of data availability and associated accession codes are available at https://doi.org/10.1038/s41567-019-0436-5.

Received: 31 August 2018; Accepted: 17 January 2019;
Published online: 25 February 2019

References

1. Spaun, B. et al. Continuous probing of cold complex molecules with infrared frequency comb spectroscopy. *Nature* **533**, 517–520 (2016).
2. Truppe, S. et al. Molecules cooled below the Doppler limit. *Nat. Phys* **13**, 1173–1176 (2017).
3. Lidzey, D. G., Bradley, D. D. C., Armitage, A., Walker, S. & Skolnick, M. S. Photon-mediated hybridization of Frenkel excitons in organic semiconductor microcavities. *Science* **288**, 1620–1623 (2000).
4. Hakala, T. K. et al. Vacuum Rabi splitting and strong-coupling dynamics for surface-plasmon polaritons and rhodamine 6G molecules. *Phys. Rev. Lett.* **103**, 053602 (2009).
5. Schwartz, T., Hutchison, J. A., Genet, C. & Ebbesen, T. W. Reversible switching of ultrastrong light–molecule coupling. *Phys. Rev. Lett.* **106**, 196405 (2011).
6. Chikkaraddy, R. et al. Single-molecule strong coupling at room temperature in plasmonic nanocavities. *Nature* **535**, 127–130 (2016).
7. Polisseni, C. et al. Stable, single-photon emitter in a thin organic crystal for application to quantum-photonic devices. *Opt. Express* **24**, 5615–5627 (2016).
8. Zhang, Y. et al. Sub-nanometre control of the coherent interaction between a single molecule and a plasmonic nanocavity. *Nat. Commun.* **8**, 15225 (2017).
9. Skoff, S. M., Papencordt, D., Schauffert, H., Bayer, B. C. & Rauschenbeutel, A. Optical-nanofiber-based interface for single molecules. *Phys. Rev. A* **97**, 043839 (2018).
10. Liu, L. R. et al. Building one molecule from a reservoir of two atoms. *Science* **360**, 900–903 (2018).
11. Moerner, W., Orrit, M., Wild, U. & Basché, T. (eds) *Single-Molecule Optical Detection, Imaging and Spectroscopy* (Wiley, New York, 1996).
12. Pototschnig, M. et al. Controlling the phase of a light beam with a single molecule. *Phys. Rev. Lett.* **107**, 063001 (2011).
13. Maser, A., Gmeiner, B., Utikal, T., Götzinger, S. & Sandoghdar, V. Few-photon coherent nonlinear optics with a single molecule. *Nat. Photon.* **10**, 450–453 (2016).
14. Kühn, S., Håkanson, U., Rogobete, L. & Sandoghdar, V. Enhancement of single-molecule fluorescence using a gold nanoparticle as an optical nanoantenna. *Phys. Rev. Lett.* **97**, 017402 (2006).
15. Berman, P. R. (ed.) *Cavity Quantum Electrodynamics* (Academic Press, San Diego, 1994).
16. Norris, D. J., Kuwata-Gonokami, M. & Moerner, W. E. Excitation of a single molecule on the surface of a spherical microcavity. *Appl. Phys. Lett.* **71**, 297–299 (1997).
17. Steiner, M., Hartschuh, A., Korlacki, R. & Meixner, A. J. Highly efficient, tunable single photon source based on single molecules. *Appl. Phys. Lett.* **90**, 183122 (2007).
18. Chizhik, A. et al. Tuning the fluorescence emission spectra of a single molecule with a variable optical subwavelength metal microcavity. *Phys. Rev. Lett.* **102**, 073002 (2009).
19. Wang, D. et al. Coherent coupling of a single molecule to a scanning Fabry–Perot microcavity. *Phys. Rev. X* **7**, 021014 (2017).
20. Toninelli, C. et al. A scanning microcavity for in situ control of single-molecule emission. *Appl. Phys. Lett.* **97**, 021107 (2010).
21. Kelkar, H. et al. Sensing nanoparticles with a cantilever-based scannable optical cavity of low finesse and sub-λ^3 volume. *Phys. Rev. Appl.* **4**, 054010 (2015).
22. Nicolet, A. A. L., Hofmann, C., Kol'chenko, M. A., Kozankiewicz, B. & Orrit, M. Single dibenzoterrylene molecules in an anthracene crystal: spectroscopy and photophysics. *ChemPhysChem* **8**, 1215–1220 (2007).
23. Trebbia, J.-B., Ruf, H., Tamarat, P. & Lounis, B. Efficient generation of near infra-red single photons from the zero-phonon line of a single molecule. *Opt. Express* **17**, 23986–23991 (2009).
24. Petermann, K. Calculated spontaneous emission factor for double-heterostructure injection lasers with gain-induced waveguiding. *IEEE J. Quantum Electron.* **15**, 566–570 (1979).
25. Auffèves-Garnier, A., Simon, C., G,rard, J. M. & Poizat, J. P. Giant optical nonlinearity induced by a single two-level system interacting with a cavity in the Purcell regime. *Phys. Rev. A* **75**, 053823 (2007).
26. Heinzen, D. J. & Feld, M. S. Vacuum radiative level shift and spontaneous-emission linewidth of an atom in an optical resonator. *Phys. Rev. Lett.* **59**, 2623–2626 (1987).
27. Cohen-Tannoudji, C., Dupont-Roc, J. & Grynberg, G. *Atom–Photon Interactions* (Wiley, Weinheim, 2004).
28. Choi, Y. et al. Quasieigenstate coalescence in an atom–cavity quantum composite. *Phys. Rev. Lett.* **104**, 153601 (2010).
29. Rice, P. R. & Carmichael, H. J. Single-atom cavity-enhanced absorption. I: Photon statistics in the bad-cavity limit. *IEEE J. Quantum Electron.* **24**, 1351–1366 (1988).
30. Ourjoumtsev, A. et al. Observation of squeezed light from one atom excited with two photons. *Nature* **474**, 623–626 (2011).
31. Schulte, C. H. H. et al. Quadrature squeezed photons from a two-level system. *Nature* **525**, 222–225 (2015).
32. Ficek, Z. & Swain, S. *Quantum Interference and Coherence: Theory and Experiments* (Springer Science + Business Media, Berlin, 2005).
33. Carmichael, H. J. & Rice, P. R. Quantum interference and collapse of the wavefunction in cavity QED. *Opt. Commun.* **82**, 73–79 (1991).
34. Bennett, A. J. et al. A semiconductor photon-sorter. *Nat. Nanotechnol.* **11**, 857–860 (2016).
35. Snijders, H. et al. Purification of a single-photon nonlinearity. *Nat. Commun.* **7**, 12578 (2016).
36. Wrigge, G., Gerhardt, I., Hwang, J., Zumofen, G. & Sandoghdar, V. Efficient coupling of photons to a single molecule and the observation of its resonance fluorescence. *Nat. Phys.* **4**, 60–66 (2008).
37. Chang, D. E., Vuletić, V. & Lukin, M. D. Quantum nonlinear optics—photon by photon. *Nat. Photon.* **8**, 685–694 (2014).
38. Rezus, Y. L. A. et al. Single-photon spectroscopy of a single molecule. *Phys. Rev. Lett.* **108**, 093601 (2012).
39. Kok, P. & Lovett, B. *Introduction to Optical Quantum Information Processing* (Cambridge Univ. Press, Cambridge, 2010).
40. Ralph, T., Söllner, I., Mahmoodian, S., White, A. & Lodahl, P. Photon sorting, efficient Bell measurements, and a deterministic controlled-Z gate using a passive two-level nonlinearity. *Phys. Rev. Lett.* **114**, 173603 (2015).
41. Rotenberg, N. et al. Small slot waveguide rings for on-chip quantum optical circuits. *Opt. Express* **25**, 5397–5414 (2017).
42. Türschmann, P. et al. Chip-based all-optical control of single molecules coherently coupled to a nanoguide. *Nano Lett.* **17**, 4941–4945 (2017).
43. Diniz, I. et al. Strongly coupling a cavity to inhomogeneous ensembles of emitters: potential for long-lived solid-state quantum memories. *Phys. Rev. A* **84**, 063810 (2011).
44. Haakh, H. R., Faez, S. & Sandoghdar, V. Polaritonic normal-mode splitting and light localization in a one-dimensional nanoguide. *Phys. Rev. A* **94**, 053840 (2016).
45. Walser, A., Zumofen, G., Renn, A., Götzinger, S. & Sandoghdar, V. Spectral dynamics and spatial localization of single molecules in a polymer. *Mol. Phys.* **107**, 1897–1909 (2009).
46. Kozyryev, I. et al. Sisyphus laser cooling of a polyatomic molecule. *Phys. Rev. Lett.* **118**, 173201 (2017).

Acknowledgements

The authors thank J. Renger, A. Dutschke and E. Butzen for the fabrication of micromirrors, M. Schwab for the construction of the mechanical components for

the cryostats, and L. Meier for help with electronics to lock the cavity. This work was supported by the Max Planck Society.

Author contributions

D.W. and H.K. performed the cavity experiments and analysed the data. D.R. and A.S. were responsible for the generation of single photons. T.U., S.G. and V.S. supervised the experiments. D.M.-C. contributed to theoretical analysis of the system. The manuscript was written by V.S. and all authors commented on it.

Competing interests

The authors declare no competing interests.

Additional information

Supplementary information is available for this paper at https://doi.org/10.1038/s41567-019-0436-5.

Reprints and permissions information is available at www.nature.com/reprints.

Correspondence and requests for materials should be addressed to V.S.

Journal peer review information: *Nature Physics* thanks Girish Agarwal, Barak Dayan and the other anonymous reviewer(s) for their contribution to the peer review of this work.

Methods

Microcavity assembly. To couple DBT molecules to a cavity mode, we placed an AC crystal with a thickness of about 600 nm weakly doped with DBT on a planar distributed Bragg reflector against a curved micromirror, forming a Fabry–Perot microcavity (Fig. 1b). The planar mirror was mounted on a slip-stick piezoelectric slider (PES: ANPz51, Attocube Systems), which positioned the AC crystal in the lateral direction. The micromirror with a radius of curvature of 10 µm was fabricated on the cleaved end of a single-mode fibre by focused ion beam (FIB) milling. A dielectric coating with 12 alternating Nb_2O_5 and SiO_2 bilayers was produced on the micromirror, reaching a total thickness of 2.7 µm and a nominal reflectivity of 99.996% to match that of the planar mirror. In Fig. 1c, a scanning electron microscope micrograph of a cut through a micromirror presents an insight into the high coating quality. The challenges in achieving such a coating are discussed in ref. [47]. The micromirror was located on a second PES (ANPx51), which travelled along the axial direction of the cavity and allowed coarse adjustment of the cavity length. Each cavity mirror was mounted on a ring piezo element to facilitate fine tuning of the cavity resonance. The incident laser beam was coupled to the cavity using an aspheric lens (352240-B, Thorlabs), which was mounted on a third PES (ANPx51) to adjust the focus of the incoming beam. A second aspheric lens (AL1225H-B, Thorlabs) was aligned after the transmission port of the fibre to collimate the transmitted light through the fibre and guide it out of the cryostat. The anthracene-filled microcavity had an optical length of 4.7 µm, a cavity mode volume of $4.4\lambda^3$, a finesse of 19,000 and a Q factor of 230,000. When placed in our helium exchange gas cryostat at 4 K, residual vibrations broadened the line. This resulted in $Q = 120{,}000$, deduced from the FWHM $\kappa/2\pi = 3.3$ GHz of a Voigt profile, which was composed of a Lorentzian resonance of FWHM = 1.7 GHz and a Gaussian broadening of FWHM = 2.3 GHz (see Supplementary Information).

Optical set-up and measurements. As shown in Fig. 1d, a Ti:sapphire laser (SolsTis, M Squared Laser) operating at 783 nm and a diode laser (DL Pro, Toptica Photonics) at 759 nm were combined at a beamsplitter and sent to the cavity via a common beam path. After being reflected from the cavity, the two laser beams were separated using a beamsplitter and two narrowband interference filters. The reflected beam of the diode laser was split by a polarizing beamsplitter and detected by a balanced photodetector to provide an error signal for active stabilization of the cavity[19,48]. The reflected beam from the Ti:sapphire laser was sent to an avalanche photodiode for the spectral measurements, or to a Hanbury Brown and Twiss (HBT) set-up for the intensity correlation measurements, controlled by a flip mirror. The strong birefringence of the AC crystal lifts the mode degeneracy for orthogonal polarizations and allows direct access to the intracavity field via detection in a cross-polarized configuration[19]. To achieve this, a polarizer, a half-waveplate and a quarter-waveplate were placed in front of the flip mirror to filter out the uncoupled reflection from the planar mirror.

In the second laboratory, a DBT-doped AC crystal placed on a fused-silica substrate with structured indium tin oxide micro-electrodes was cooled to 1.4 K in a second cryostat. The light from a second Ti:sapphire laser (SolsTis, M Squared Laser) at 765 nm was focused on the sample to excite the 'source' molecule to a higher vibrational level of its electronic excited state. The emission at the 00ZPL was collected with an aspheric lens, and spectrally separated from other redshifted emissions and the excitation light using a bandpass filter. The 00ZPL emission was first sent to an HBT set-up to confirm its single-photon nature via an intensity correlation measurement. The 00ZPL emission was then coupled to a single-mode fibre and guided to the cryostat hosting the microcavity. The single photon stream was coupled out of the fibre in the main laboratory and passed through a half-waveplate to align its polarization to that of the cavity mode. A beamsplitter was used to send 50% of the photons to the cryostat, where they were focused by an aspheric lens and coupled to the cavity.

Phase shift measurement. We used a two-frequency common-path interferometer as described in ref. [12] to measure the phase shift of the transmitted light. A laser beam was sent to an acousto-optic modulator (EF 300–200, Brimrose) driven at an acoustic frequency of 330 MHz. After passing through the acousto-optic modulator, the fundamental (zeroth) and second diffraction order, which are frequency separated by twice the acoustic frequency, were selected and combined at a beamsplitter. The combined beam was coupled to a single-mode fibre that guided the light to the experiment. Before the beam was sent to the cavity, a beam sampler reflected part of the intensity to a fast avalanche photodiode (APD210, Menlo Systems). The sinusoidal signal measured by the detector was fed to a time-correlated single-photon counting (TCSPC) device (Picoharp300, PicoQuant) to serve as a trigger signal. The frequency of the Ti:sapphire laser was tuned across the resonance of the coupled system, while the arrival time of the transmitted photons with respect to its previous trigger event was recorded by the TCSPC device. At each laser frequency, a histogram of the time delay of the photon detection events was generated. A sinusoidal fit to each of the histograms was performed to extract the starting phase of the beating signal. The phase of the beating signals was plotted against the laser frequency and fitted to theory to obtain the system parameters and the phase shift on a single beam. See Supplementary Information for details.

Data availability

The data that support the plots within this paper and other findings of this study are available from the corresponding author upon reasonable request.

References

47. Trichet, A. A. P., Dolan, P. R., Coles, D. M., Hughes, G. M. & Smith, J. M. Topographic control of open-access microcavities at the nanometer scale. *Opt. Express* **23**, 17205–17216 (2015).
48. Hänsch, T. W. & Couillaud, B. Laser frequency stabilization by polarization spectroscopy of a reflecting reference cavity. *Opt. Commun.* **35**, 441–444 (1980).